

Inverse estimation of impact force on a composite panel using a single piezoelectric sensor

Hamed Kalhori¹, Lin Ye¹ and Samir Mustapha²

Journal of Intelligent Material Systems and Structures
2017, Vol. 28(6) 799–810
© The Author(s) 2016
Reprints and permissions:
sagepub.co.uk/journalsPermissions.nav
DOI: 10.1177/1045389X16657424
journals.sagepub.com/home/jim



Abstract

Identification of location and magnitude of impact forces on a rectangular carbon fibre–epoxy honeycomb composite panel has been experimentally investigated through an inverse approach. The dynamic signals captured by a single piezoelectric (PZT) sensor installed on the panel remotely from the impact locations are utilized to identify the impact forces generated by an instrumented hammer. A number of potential impact locations on the panel are assumed to be known a priori. An actual impact is then occurred at one or two of these locations. The objective is to simultaneously identify the location and magnitude of the impact forces using the PZT sensor. The problem is solved through minimization of an extended matrix form of the convolution integral incorporating linear superposition of the responses due to impact at different locations. The under-determined problem is ill-posed and is regularized by Tikhonov and generalized cross validation methods. It is revealed that impact forces occurred at any location among four possible locations can be well identified.

Keywords

Impact force estimation, inverse problem, honeycomb composite panel, piezoelectric

Introduction

Composite structures extensively used in aerospace industries are exposed to various types of barely visible impact failure including de-bonding of core and skins, delamination of carbon fibre or epoxy laminate skins and deformation of honeycomb core in sandwich structures. The vital importance of structural health monitoring (SHM) systems can be well realized by looking at their effective contribution towards safety improvement of aircraft structures since a considerable portion of their entire structures is composed of composite materials (Staszewski et al., 2009).

SHM can be performed in active mode, that is, direct assessment through a scheduled time-based monitoring scheme or passive mode, that is, indirect assessment through a condition-based inspection technique (Giurgiutiu, 2003, 2005; Giurgiutiu et al., 2001; Ihn and Chang, 2008; Li et al., 2015; Staszewski et al., 2009). Active SHM system utilizes both actuators and sensors, whereas passive SHM system uses only sensors to detect the events such as any impact, crack or damage. Time-based monitoring techniques suffer from some drawbacks resulting in inconvenience and inefficiencies in evaluation process (Choi and Chang, 1996; Jang et al., 2012; Park et al., 2009). Localization of the

inspection area for only high-energy impacts will compensate for some of the disadvantages associated with active SHM system. Therefore, an automatic system to detect impact occurrence together with both impact location and its magnitude would enhance the efficiency of SHM systems for damage prediction.

Extensive studies have been done on impact force identification for composite panels using model-based techniques which are based on properties and dynamic characteristics of the structure (Hu et al., 2007b; Mao et al., 2010; Seydel and Chang, 2001a, 2001b; Tracy and Chang, 1996, 1998). Transfer functions for complicated composite structures representing their dynamic behaviour can be built either by finite element methods (Hu et al., 2007a) or experimental approach (Kalhori

¹Laboratory of Smart Materials and Structures (LSMS), School of Aerospace, Mechanical and Mechatronic Engineering, The University of Sydney, Sydney, NSW, Australia

²Department of Mechanical Engineering, American University of Beirut, Beirut, Lebanon

Corresponding author:

Lin Ye, Laboratory of Smart Materials and Structures (LSMS), School of Aerospace, Mechanical and Mechatronic Engineering, The University of Sydney, Sydney, NSW 2006, Australia.
Email: l.ye@usyd.edu.au

et al., 2014, 2016) Non-model-based techniques utilizing neural networks have also attracted much attention for impact identification in composite structures (Akhavan et al., 2000; Jang et al., 2012; Worden and Staszewski, 2000). Most of the composite panels would produce impact forces with different patterns when exposed to various impactors with different properties. As a result, to confidently apply neural networks to real applications, massive training data must be collected which is a downside (Park et al., 2009).

Impact force magnitude is usually calculated by creating an optimization model to minimize the difference between the measured and predicted dynamic responses. The created model is usually very sensitive to perturbations. The ill-posed nature of the governing equation, that is, transfer function, of the system does not allow for a converged and steady force reconstruction. Several regularization methods including Tikhonov, truncated singular value decomposition (TSVD), damped SVD and iterative regularization methods were proposed to surmount the difficulties associated with the ill-posed problems (Hansen, 1994, 1998). B-spline scaling functions were also adopted for regularization of impact force reconstruction problems (Gunawan et al., 2006; Qiao et al., 2015). Gaussian kernel smoothing has been also applied as a regularization operator to enhance the signal-to-noise ratio (Alamdari et al., 2014).

For a simple structure with known wave speed in all directions such as an isotropic metallic plate, impact location can be identified using a triangulation technique (Kundu et al., 2007). However, it is problematic to differentiate the exact arrival time of impact response captured by sensors from the raw signal. This is because the wave produced by impact is dispersive and so the initial portion of the impact response is of low amplitude and high frequency (Tracy and Chang, 1998). A modified triangulation procedure utilizing experimentally obtained velocities and an optimization method was proposed for impact location identification for anisotropic materials (Coverley and Staszewski, 2003). Neural networks were also used to identify the impact location (Akhavan et al., 2000). These methods are capable of producing accurate estimation of impact location for even complicated structures. However, as mentioned previously, enormous training data needed which sometimes is impractical in actual applications (Staszewski et al., 2009). A new approach utilizing neural networks together with trilateration was also implemented to find impact location at reduced computational cost (De Stefano et al., 2015). Minimization of the difference between the calculated responses and the measured ones using optimization algorithms was also adopted for impact location identification (Choi and Chang, 1996; Hu et al., 2007a). In addition to the above-mentioned methods, proper orthogonal decomposition which is a statistical method was used to

identify impact location on a composite plate (Thiene and Galvanetto, 2015). Recently, a method was adopted to concurrently identify both impact location and magnitude on a lattice truss core composite panel through an even-determined problem which utilizes the dynamic responses captured by a scanning laser Doppler vibrometer (Kalthori et al., 2015).

In this study, an inverse method was developed to estimate the location and magnitude of impact forces exerted to a rectangular carbon fibre–epoxy honeycomb composite sandwich panel. Deconvolution, usually applied to reconstruct the time history (e.g. magnitude) of a stochastic force at a defined location, is extended to identify both the location and magnitude of the impact force among a number of potential impact locations. It is supposed that a number of impact forces are simultaneously exerted to all potential locations, but the magnitude of all forces except one is zero, implicating that the impact occurs only at one location. It comprises four potential impact locations and one PZT sensor on a rectangular carbon fibre–epoxy composite honeycomb sandwich panel. The matrix form of the convolution integral incorporates the linear superposition of the responses due to the ‘assumed’ impact at all potential locations. The problem is solved through minimizing the predicted and captured dynamic responses. Tikhonov regularization is chosen to regularize the problem, and the generalized cross validation (GCV) method is used to find the optimal value of the regularization parameter. The application of the proposed method for identification of concurrent impacts at multiple locations was also investigated.

Formulation of the problem

In a linear system, the vibration response, for example, dynamic strain ε recorded at point ζ due to a stochastic force f exerted at location ϑ can be represented by a convolution integral as (Inman, 2001)

$$\varepsilon(\zeta, t) = \int_0^t k(\vartheta, \zeta, t - \tau) f(\vartheta, \tau) d\tau \quad (1)$$

where $k(\vartheta, \zeta, t - \tau)$ is the transfer function in the time domain between impact location ϑ and measurement point ζ , which can be defined using an inverse algorithm (Inoue et al., 2001). The discretized form of the convolution integral is given by a system of algebraic equations as

$$\varepsilon_z = \sum_{i=0}^{z-1} k_{i+1} f_{z-i}, \quad (z = 1, \dots, p) \quad (2)$$

Equation (2) can be expressed in matrix form as $[E] = [K][F]$ where

$$[K] = \begin{bmatrix} k_1 & 0 & \cdots & \cdots & 0 \\ k_2 & k_1 & \ddots & \ddots & \vdots \\ k_3 & k_2 & \ddots & \ddots & \vdots \\ \vdots & \vdots & \ddots & \ddots & 0 \\ k_p & k_{p-1} & \cdots & \cdots & k_1 \end{bmatrix}, [E] = \begin{Bmatrix} \varepsilon_1 \\ \varepsilon_2 \\ \varepsilon_3 \\ \vdots \\ \varepsilon_p \end{Bmatrix},$$

$$[F] = \begin{Bmatrix} f_1 \\ f_2 \\ f_3 \\ \vdots \\ f_p \end{Bmatrix} \quad (3)$$

where k_z ($z = 1, \dots, p$) is the value of transfer function at time $t_z = z \cdot \Delta t$ and p is the number of samples.

Assuming a number of impact forces at different locations F_i ($i = 1, \dots, Q$) simultaneously applied to a structure, the corresponding dynamic strain signal at a given measurement point E_j ($j = 1, \dots, H$) is a superposition of the responses caused by each single force

$$E_j = K_j^1 F_1 + K_j^2 F_2 + \cdots + K_j^Q F_Q = \sum_{i=1}^Q K_j^i F_i \quad (4)$$

where K_j^i is the transfer function between force location i and measurement point j . For a single measurement point, equation (4) can be expressed as

$$[E] = [K^1 \quad K^2 \quad \cdots \quad K^Q] \begin{bmatrix} F_1 \\ F_2 \\ \vdots \\ F_Q \end{bmatrix} \quad (5)$$

where Q and H represent the number of impact locations and measurement points, respectively. For brevity, equation (5) is presented by $E = KF$. The solution is then obtained using the least squares problem as

$$\min \|E - KF\|_2^2 \quad (6)$$

where E practically is an error-contaminated vector and K is a matrix with many singular values of different orders of magnitude. Minimization problem (6) with a matrix of this kind often is referred to as a discrete ill-posed problem. Let e denote the error in E , and let \tilde{E} be the error-free vector associated with E . So

$$E = \tilde{E} + e \quad (7)$$

The desired purpose is to define F of the unattainable linear system ($F = K^\dagger \tilde{E}$) by determining an approximate solution of the existing least squares problem, that is, equation (6). Matrix K^\dagger is the Moore–Penrose pseudo-inverse of K . The solution of equation (6) is given by

$$F = K^\dagger E = K^\dagger (\tilde{E} + e) = \tilde{F} + K^\dagger e \quad (8)$$

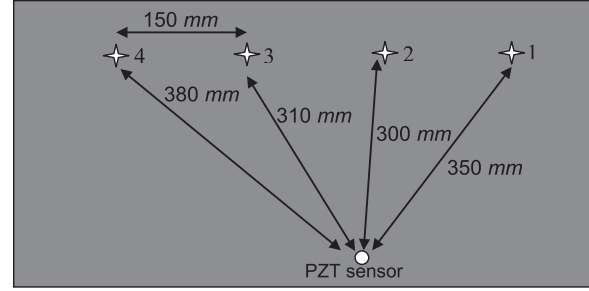


Figure 1. Impact locations (\star) on the panel with respect to location of a PZT disc sensor.

which normally does not generate a meaningful approximation of \tilde{F} . Tikhonov regularization pursues to determine a good approximation of \tilde{F} , which replacing the problem (6) by a penalized least squares problem of the form

$$\min \left\{ \|E - KF\|_2^2 + \delta \|IF\|_2^2 \right\} \quad (9)$$

where I is the identity matrix and $\delta \geq 0$ is the regularization parameter which can be determined by the GCV method (Hansen, 1994). The term $\delta \|IF\|_2^2$ in equation (9) actually attenuates the effect of $K^\dagger e$ in equation (8).

Experimental set-up and procedure

A composite sandwich panel (600 mm in length and 400 mm in width) was manufactured using carbon fibre laminates consisting of four woven plies in a quasi-isotropic lay-up $[\pm 45, 0/90]_s$ with a nominal thickness of 0.88 mm and a honeycomb core of 20 mm thickness. The core is made out of Nomex material which is a non-woven sheet made of short aramid fibres (Mustapha et al., 2016). The face sheets were initially cured in an autoclave following the recommended procedure. The skins and core were then assembled together with FM 1515-3 film adhesive (Liljedahl et al., 2008) using secondary bonding, which were achieved in the autoclave at the recommended temperature and low pressure to avoid crushing the core. The manufacturing process of the composite panel was described in details in Mustapha and Ye (2014, 2015) and Mustapha et al. (2012). The panel was clamped at two opposite edges and free at the other two edges during experiments.

A circular PZT element (PIC 151, PQYY + 0221) with a diameter of 10 mm and a thickness of 1 mm was surface mounted on the composite panel using Loctite Super Glue at the point shown in Figure 1. The PZT sensor actually measures the strain invariant $\varepsilon = \varepsilon_{xx} + \varepsilon_{yy}$. The output voltage V_{out} captured by the PZT sensor is related to strain invariant by

$$V_{out} = \frac{(\varepsilon_{xx} + \varepsilon_{yy})}{C} \quad (10)$$

where C is a constant depending on sensor thickness, piezoelectric coefficient and the bonding effects (Peelamedu et al., 2005). If the wavelength of the dynamic signals is assumed to be much longer than the sensor diameter, the sensor response can be considered as a point response.

Impact was applied using an instrumented hammer (Meggitt's Endeveco, 2303) at four potential impact locations distributed along a line on the panel as depicted in Figure 1. The distance of impact locations to the PZT sensor is in the range of $30 \text{ mm} < d < 38 \text{ mm}$, where d is the distance between the sensor and impact location. The signals measured by the PZT sensor and the modal hammer were collected using an oscilloscope (Tektronix DPO4034B). Figure 2 illustrates the experimental set-up. The signal acquisition was triggered as soon as the impact force by the hammer surpassed a small certain value (20 N) and was sampled at a rate of 50 kHz.

Identification of location and magnitude

To establish the transfer function between each impact location and the PZT sensor, a reference impact force was first exerted at each impact location individually and the corresponding dynamic signals are captured by the PZT sensor. The steps for establishing the transfer function was discussed in detail in previous studies (Kalhori et al., 2014; Kalhori et al., 2016). In addition, to avoid any possible dent or damage, the magnitude of applied forces for both the transfer function establishment and later impact force identification was limited not to exceed 500 N. Figure 3 illustrates some typical magnitude of impact forces applied at locations 1–4 for transfer function establishment, which were captured by the load sensor inside the instrumented hammer.

It is supposed that four impact forces are concurrently applied at the demarcated impact locations as in Figure 1, but the magnitude of all forces except one is zero, implicating that the impact takes place only at one location. As a result, the problem is under-determined since it encompasses one known (strain response by the piezoelectric sensor) and four unknowns (impact forces at four locations). As a case study, the impact is applied at location 3. Two different cases are investigated. First, all four impact locations are taken into account as the potential impact locations. Second, the potential impact locations are just three out of the four, with four groups, that is, locations 1, 2 and 3; locations 1, 3 and 4; locations 1, 2 and 4; and locations 2, 3 and 4.

The reconstructed force at each location using the algorithms discussed in the previous section is assessed addressing key characteristics of a normal impact force such as the shape, the maximum amplitude of the first peak if applicable and the momentum change of the

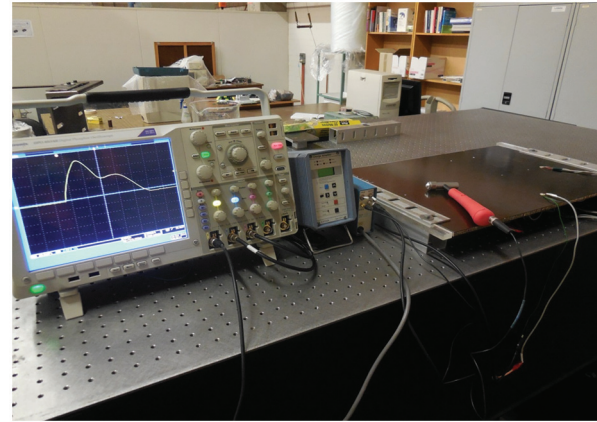


Figure 2. Experimental set-up including the impact hammer, signal conditioner and oscilloscope.

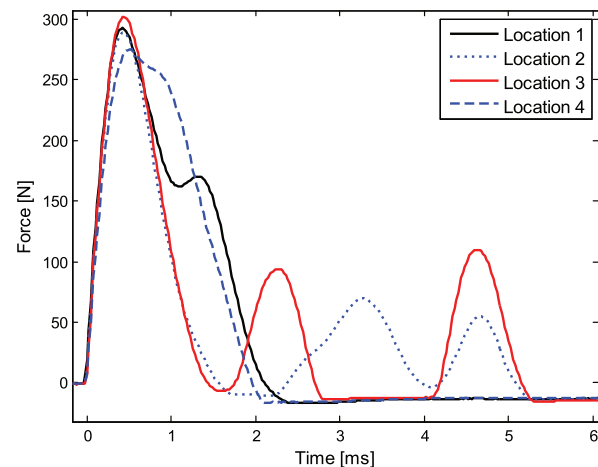


Figure 3. Impact forces applied by an impact hammer with an aluminium tip at different locations.

impactor. A typical impact force should have a smooth temple shape with or without multiple reflections. In addition, since an impact force is totally compressive, there should not be a negative portion in the reconstructed impact force. Besides, for the case of existing multiple reflections or local peaks in impact force as a result of a normal free strike, the first peak normally has a higher energy than the next peaks. Moreover, the reconstructed force at true impact location must have the higher peak amplitude among the other possible locations. It is also assumed that the reconstructed impact force starts to rise from the zero baseline.

The momentum change Δp of an object due to an application of a force F between time t_1 and t_2 can be given by (Beer et al., 1962)

$$\Delta p = \int_{t_1}^{t_2} F dt \quad (11)$$

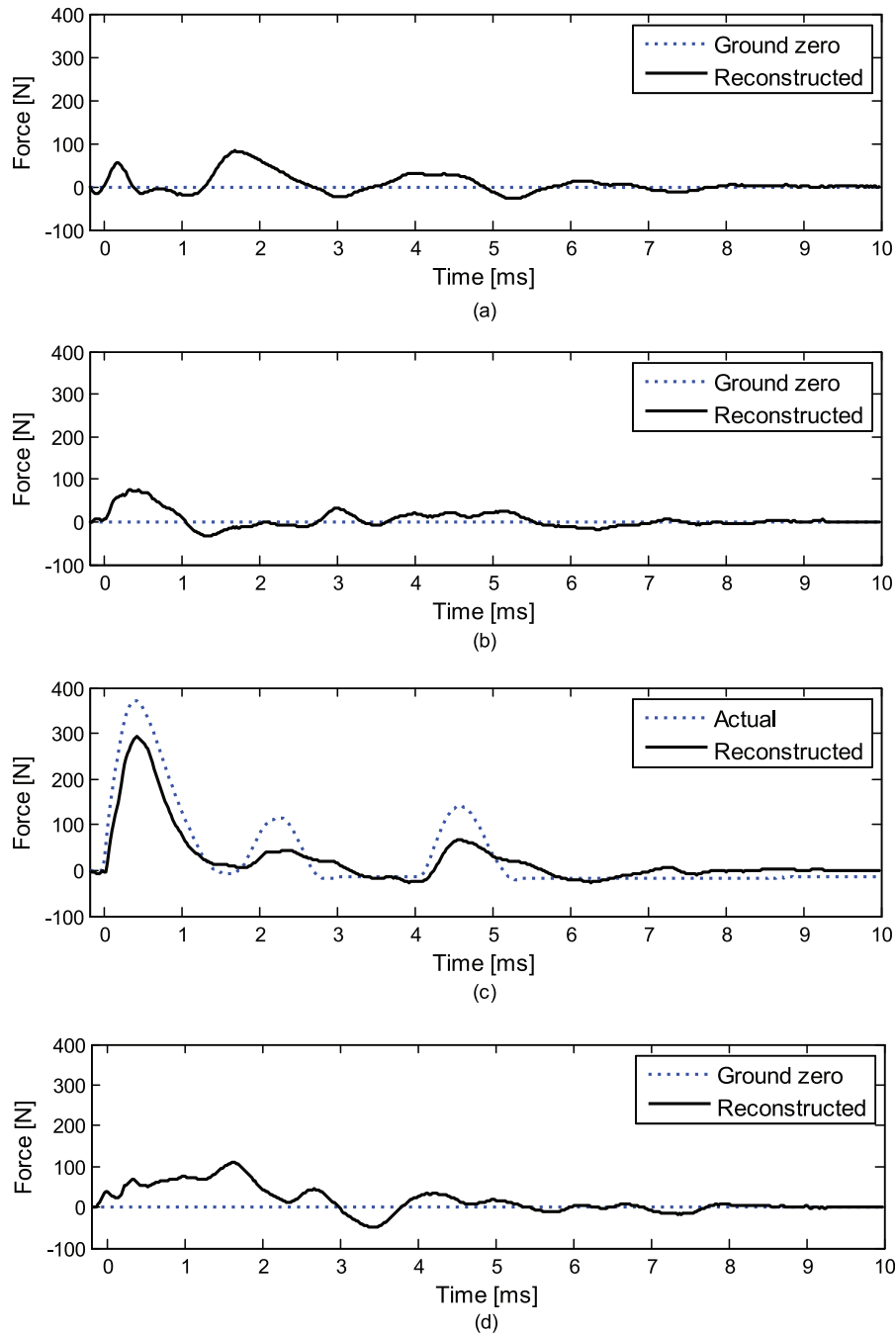


Figure 4. Reconstructed impact forces at (a) location 1, (b) location 2, (c) location 3 and (d) location 4 using dynamic signals captured by a PZT sensor.

which is to the area under the reconstructed force curve. It is envisaged that the momentum change for the reconstructed impact force at the actual impact location is much higher than that for the rest of the locations since there is no impact force at these locations.

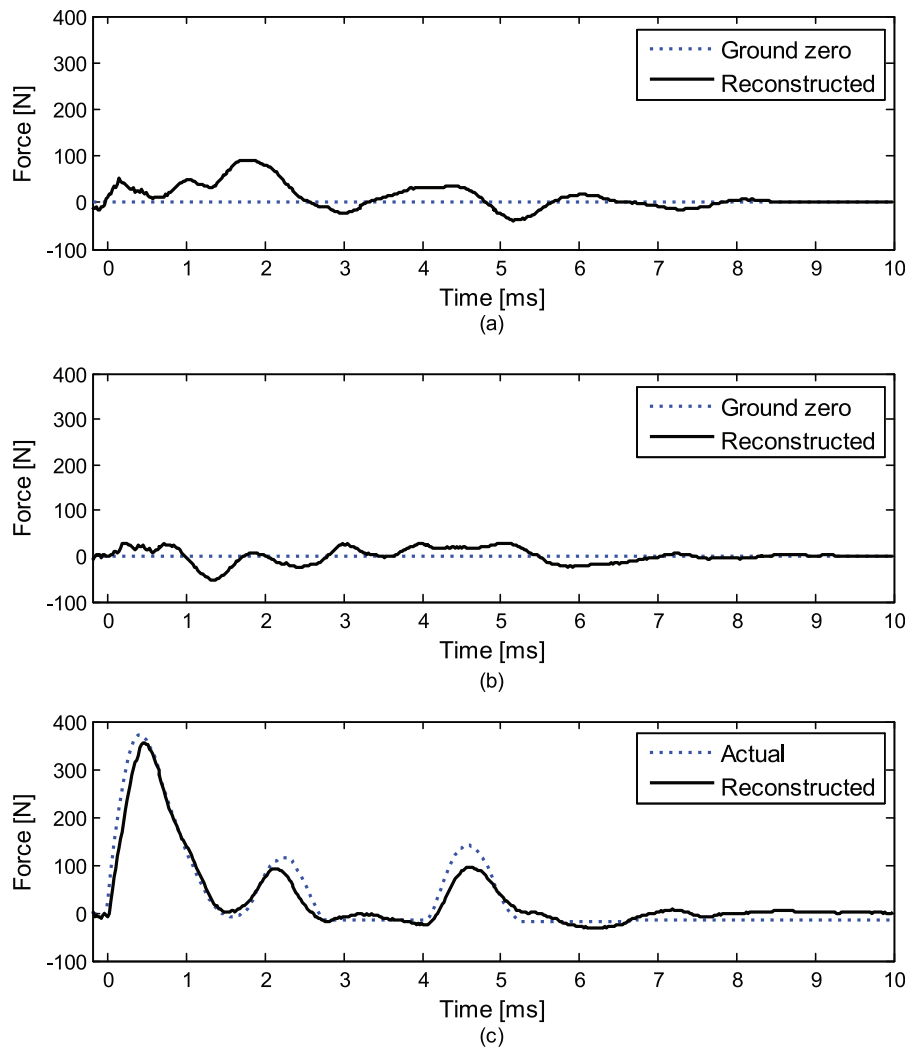
Based on these characteristics, an automated procedure can be established to identify the impact force that is the most possible one among the reconstructed forces at different locations. In the following sections, the results are articulated in addressing such a procedure.

Four possible impact locations

Figure 4 illustrates the reconstructed impact forces at four potential impact locations while the actual impact was applied at location 3. As can be seen in Figure 4 (a) and (d), the reconstructed impact forces at locations 1 and 4 do not resemble a nominal impact force. In addition, the first peak of reconstructed force at location 1 (55 N) is lower than the second peak (82.29 N); the reconstructed force amplitude at location 4 at $t = 0$ ms is above ground zero, which further confirms that

Table 1. Details of the reconstructed forces shown in Figure 4.

Potential impact location	Impact-like force	Δp (kg m/s)	Maximum amplitude (N)	Estimated location
1	×	0.068	82.29	3
2	↘	0.051	75.53	3
3	↘	0.246	292.2	3
4	×	0.162	109.7	3

**Figure 5.** Reconstructed impact forces at (a) location 1, (b) location 2 and (c) location 3 using dynamic signals measured by a PZT sensor.

locations 1 and 4 are not the actual locations at which impact occurred.

The reconstructed force at location 2 looks like a normal temple-shaped impact. However, the maximum amplitude of the reconstructed force (75.53 N) and momentum change (0.051 kg m/s) are very small compared to those of location 3, indicating that the reconstructed force at location 2 might just be as a result of noise and errors from the inverse calculations. As depicted in Figure 4(c), the reconstructed force at

location 3 resembles a nominal impact force with multiple peaks where the magnitude of the first peak is considerably higher than the other peaks. The maximum magnitude of the reconstructed force and momentum change are 292.2 N and 0.246 kg m/s, leading to errors of 27% and 35% when being compared with the actual values, respectively. Table 1 summarizes the details of the reconstructed forces. The correlation coefficient (Kalhori et al., 2016) between the reconstructed force and the actual impact force for locations 1, 2, 3 and 4

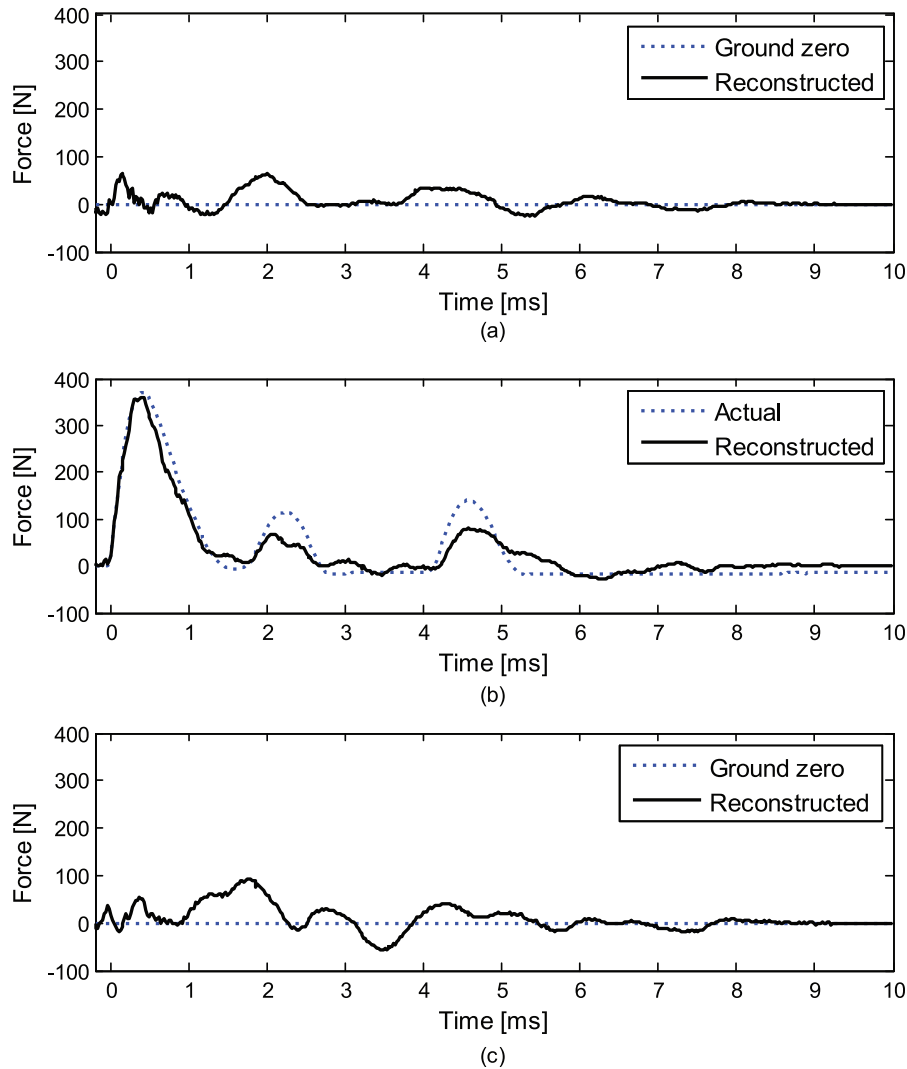


Figure 6. Reconstructed impact forces at (a) location 1, (b) location 3 and (c) location 4 using dynamic signals measured by a PZT sensor.

from $t = 0$ ms to $t = 10$ ms is 0.139, 0.737, 0.959 and 0.497, respectively, confirming that the impact force at location 3 is most likely the actual location.

Three possible impact locations

Figure 5 shows the reconstructed forces when only locations 1, 2 and 3 are taken as potential candidates for impact locations. As it can be seen, the reconstructed impact forces at locations 1 and 2 have some oscillations but with almost even magnitude. The reconstructed force at location 3 looks like an actual impact force with the maximum amplitude and momentum change of the reconstructed force being 355.8 N and 0.315 kg m/s, respectively. It apparently coincides with the actual force leading to errors of $<5\%$ and 5.5% with respect to actual values in the magnitude and momentum change, respectively. The correlation coefficient between the reconstructed force and the actual

impact force for locations 1, 2 and 3 from $t = 0$ ms to $t = 10$ ms is 0.333, 0.316 and 0.972, respectively.

Figure 6 illustrates the reconstructed impact forces at locations 1, 3 and 4. At first glance, impact locations 1 and 4 can be excluded from potential candidates since the magnitude and momentum change of the reconstructed forces at the two locations are very small compared to those of location 3. Furthermore, both the reconstructed forces have abnormal shapes with negative magnitude sometimes. This is unrealistic since an impact force is only compressive. The force at location 3 can be recognized. The maximum amplitude of the reconstructed force and momentum change at location 3 are 360.1 N and 0.331 kg m/s, respectively, leading to errors of about 4% and 1%, respectively, with respect to the actual values. The correlation coefficient between the reconstructed force and the actual impact force for locations 1, 3 and 4 from $t = 0$ ms to $t = 10$ ms is 0.317, 0.967 and 0.230, respectively.

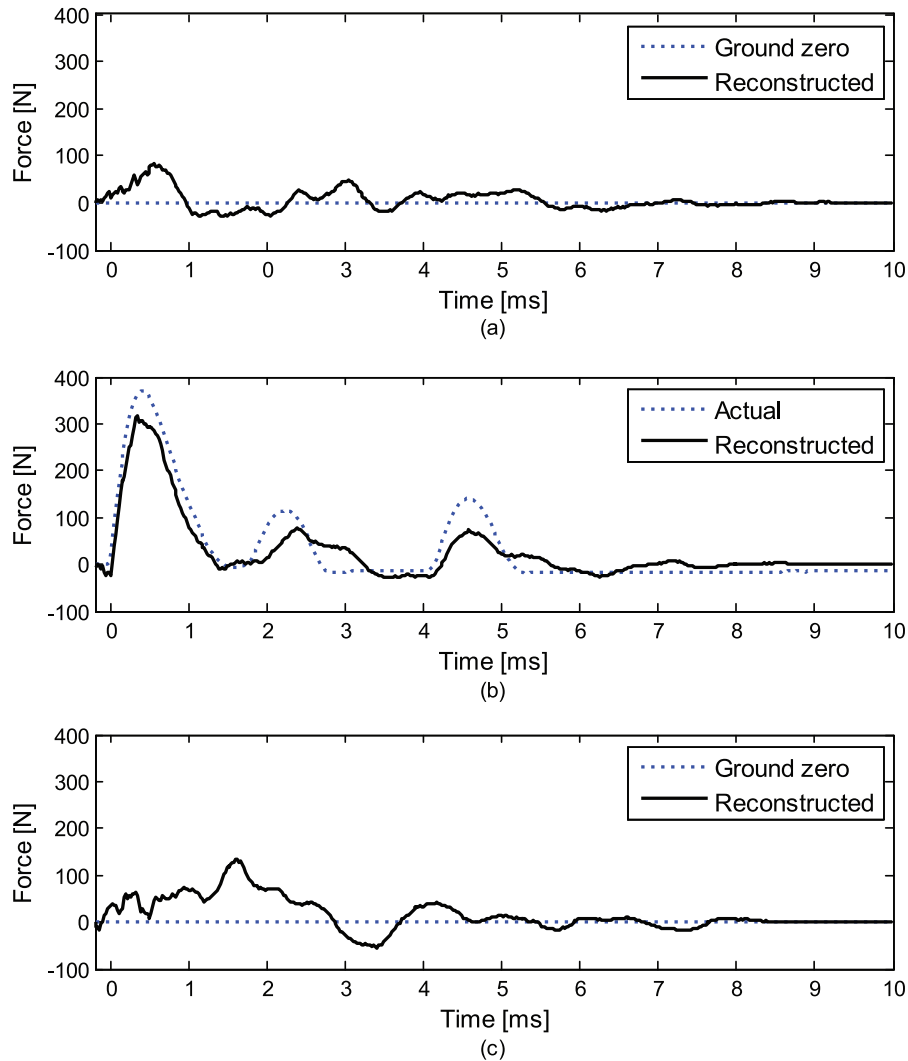


Figure 7. Reconstructed impact forces at (a) location 2, (b) location 3 and (c) location 4 using dynamic signals measured by a PZT sensor.

The reconstructed impact forces at locations 2, 3 and 4 are illustrated in Figure 7. From visual assessment, the impact forces at locations 2 and 4 are readily excluded. Despite a relatively large maximum amplitude and momentum change for location 4, it has a completely strange shape, disregarding this location as a candidate. Maximum amplitude of the reconstructed force and momentum change at location 3 are 318.4 N and 0.276 kg m/s, leading to errors of about 14% and 17% when compared to the actual values, respectively. The correlation coefficient between the reconstructed force and the actual impact force for locations 2, 3 and 4 from $t = 0$ ms to $t = 10$ ms is 0.426, 0.955 and 0.396, respectively.

It is observed that dropping the number of potential impact locations would enhance the accuracy of the reconstructed force. This is attained by comparing the errors in the maximum magnitude and momentum

change of the reconstructed impact force between the three-location problems and the four-location problem.

In Figure 8, locations 1, 2 and 4, at none of which actual impact occurred, are taken as potential impact locations. As illustrated in Figure 8(a), the reconstructed force at location 1 begins with some small peaks followed by a relatively large negative value. As mentioned previously, since the impact force is compressive, there must be no such negative (or tensile) magnitude. This reveals that location 1 is not the actual location. Similarly, the reconstructed force at location 2 includes a large negative portion, which excludes this location as a candidate. The strange shape, negative force value and non-zero amplitude at $t = 0$ s also excludes location 4 as a candidate. As can be seen, the impact force was not identified, which coincides with the fact that impact occurred at none of these locations. Therefore, if the impact occurs at a location other than

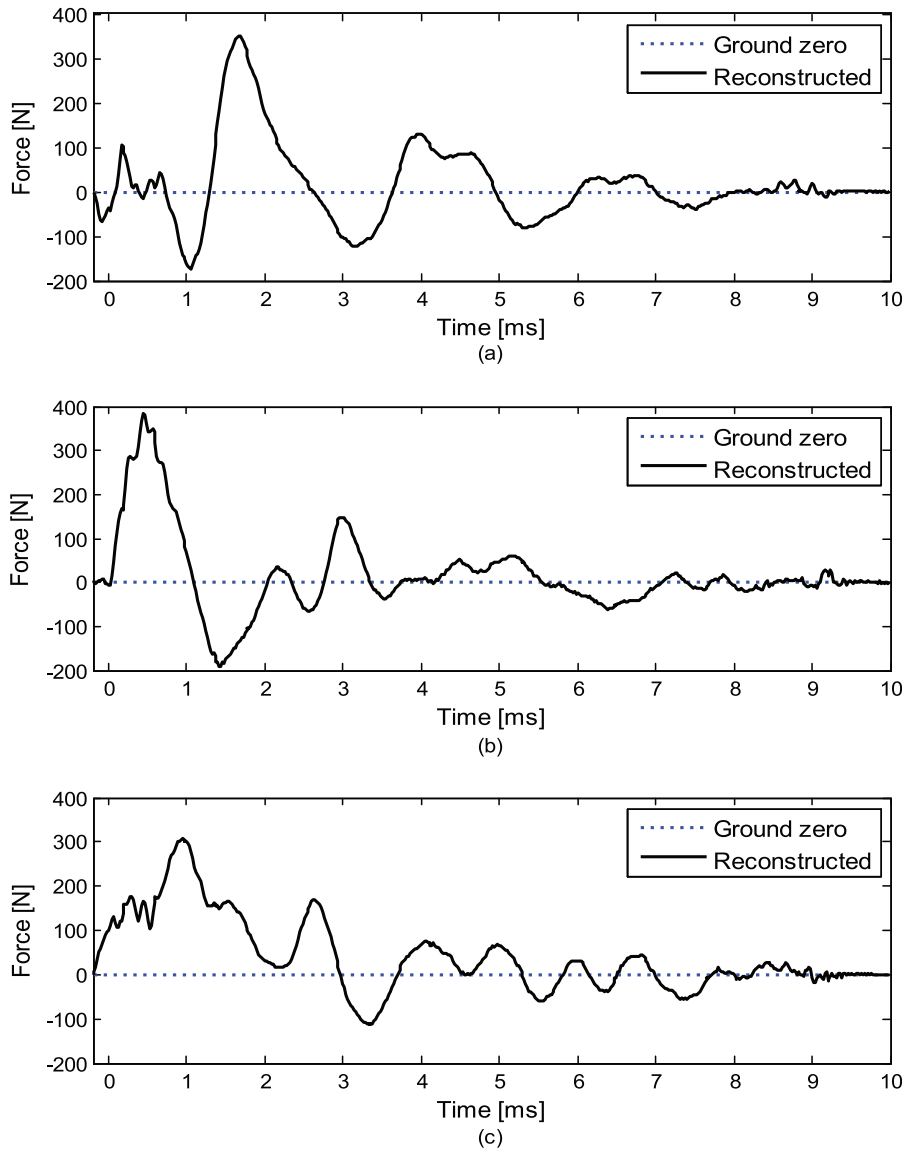


Figure 8. Reconstructed impact forces at (a) location 1, (b) location 2 and (c) location 4 using dynamic signals measured by a PZT sensor.

Table 2. Details of the reconstructed forces shown in Figures 5 to 8.

Potential impact location	Location	Impact-like force	Δp (kg m/s)	Maximum amplitude (N)	Estimated location
1, 2 and 3	1	×	0.119	91.16	3
	2	×	0.002	29.14	
	3	✓	0.315	355.8	
1, 3 and 4	1	×	0.066	65.08	3
	3	✓	0.332	360.1	
	4	×	0.097	92.03	
2, 3 and 4	2	×	0.057	82.08	3
	3	✓	0.276	318.4	
	4	×	0.162	133.2	
1, 2 and 4	1	×	NA	NA	None
	2	×	NA	NA	
	4	×	NA	NA	

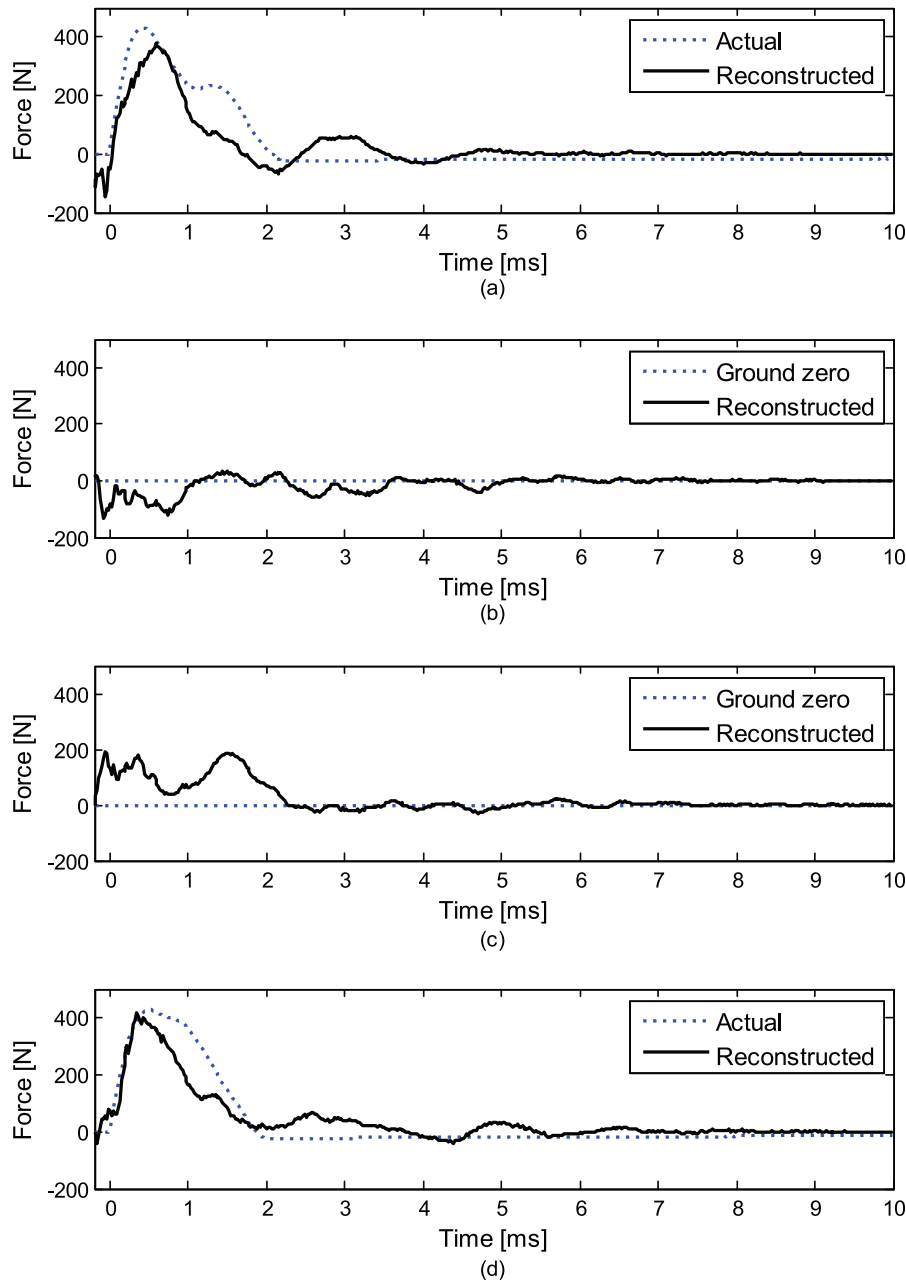


Figure 9. Identification of two concurrent impact forces at (a) location 1, (b) location 2, (c) location 3 and (d) location 4 using dynamic signals measured by a PZT sensor.

the possible candidates, the algorithm is only capable to define that the impact has occurred at none of the possible locations. In this case, the method will not be able to find the exact location. Table 2 summarizes the details of the reconstructed forces for four potential impact locations. It should be noted that the effectiveness of the algorithm decreases by increasing the number of potential impact locations. In this study, we started with a larger number of possible impact locations; it was observed that the algorithm starts to work efficiently for four possible impact locations, although the mechanism is not clear yet.

Two concurrent impact forces

Two impact forces are simultaneously applied at two of the four possible locations. The focus was on identification of impact locations together with their magnitudes. Since the exactly simultaneous application of two impacts was difficult using impact hammers, we applied the impact at two locations separately and then superimposed the responses. Based on the superposition principle, for a linear system as assumed in this study, the response at a given time produced by two or more impact forces is the summation of the responses which would have been resulted from each force individually.

Table 3. Details of the reconstructed forces shown in Figure 9.

Potential impact location	Impact-like force	Δp (kg m/s)	Maximum amplitude (N)	Estimated locations
1	✓	0.286	377.1	1 and 4
2	×	-0.120	33.28	
3	×	0.242	190.7	
4	✓	0.411	415.8	

Therefore, the obtained superimposed response was considered as a response due to two concurrent impact forces and was then fed into equation (5).

As a case study, the impacts were applied at locations 1 and 4. As can be seen in Figure 9, the impact at locations 1 and 4 was visually identifiable with the reconstructed forces of magnitudes of around 400 N. The impact force at location 2 is flat and around the ground zero indicating no impact occurred at this location. The reconstructed force at location 3 has a relatively strange shape with almost equal multiple peaks of low magnitude that are clearly lower than those at locations 1 and 4, which further helps in excluding this location as a candidate. As a result, the impact locations have been identified; however, an accurate estimation of impact magnitude was not achieved. Table 3 summarizes the details of the reconstructed forces. The correlation coefficient between the reconstructed force and the actual impact force for locations 1 and 4 from $t = 0$ ms to $t = 10$ ms is 0.877 and 0.934, respectively.

Concluding remarks

Identification of impact forces on a carbon fibre–epoxy honeycomb composite panel was investigated using an inverse approach through evaluation of dynamic signals captured by a single piezoelectric sensor. Both the location and magnitude of an impact force were simultaneously determined using the convolution principle considering the superposition of responses due to forces applied at four potential locations. Two scenarios with different numbers of potential impact locations (4 and 3) were considered. Based on the assessment factors including the shape and magnitude of the reconstructed forces, the impact location is identified as location 3 for all arrangements of potential impact locations incorporating location 3. It was also found that if the actual impact location is not among the potential locations, the reconstructed forces are all with abnormal characteristics, which can then be excluded. Furthermore, it was revealed that reducing the number of potential impact locations would increase the accuracy of the reconstructed force as a three-location problem with an arrangement of possible location lessened momentum errors to about 1%. Finally, the method was applied for identification of two concurrent impact forces. However, the shape of the reconstructed forces did not

precisely match with the actual ones, but the locations of the impact forces were clearly identified.

Declaration of conflicting interests

The author(s) declared no potential conflicts of interest with respect to the research, authorship and/or publication of this article.

Funding

The author(s) received no financial support for the research, authorship and/or publication of this article.

References

- Akhavan F, Watkins SE and Chandrashekhara K (2000) Prediction of impact contact forces of composite plates using fiber optic sensors and neural networks. *Mechanics of Composite Materials and Structures* 7: 195–205.
- Alamdari MM, Li J and Samali B (2014) FRF-based damage localization method with noise suppression approach. *Journal of Sound and Vibration* 333: 3305–3320.
- Beer FP, Johnston ER Jr, Mazurek DF, et al. (1962) *Vector Mechanics for Engineers*. New Delhi, India: Tata McGraw-Hill Education.
- Choi K and Chang F-K (1996) Identification of impact force and location using distributed sensors. *AIAA Journal* 34: 136–142.
- Coverley P and Staszewski W (2003) Impact damage location in composite structures using optimized sensor triangulation procedure. *Smart Materials and Structures* 12: 795–803.
- De Stefano M, Gherlone M, Mattone M, et al. (2015) Optimum sensor placement for impact location using trilateration. *Strain* 51: 89–100.
- Giurgiutiu V (2003) Lamb wave generation with piezoelectric wafer active sensors for structural health monitoring. In: *SPIE's 10th annual international symposium on smart structures and materials*. International society for optics and photonics, San Diego, CA, 2–6 March, pp. 111–122. Bellingham, WA: SPIE. Available at: http://www.me.sc.edu/research/lamss/pdf/conferences/c83_spie03_5056-17_numbers.pdf
- Giurgiutiu V (2005) Tuned lamb wave excitation and detection with piezoelectric wafer active sensors for structural health monitoring. *Journal of Intelligent Material Systems and Structures* 16: 291–305.
- Giurgiutiu V, Bao J and Zhao W (2001) Active sensor wave propagation health monitoring of beam and plate structures. In: *SPIE's 8th annual international symposium on*

- smart structures and materials. *International society for optics and photonics*, Newport Beach, CA, 4–8 March, pp. 234–245. Bellingham, WA: SPIE. Available at: http://www.me.sc.edu/research/lamss/pdf/conferences/c65_spie2001_4327-32.pdf
- Gunawan FE, Homma H and Kanto Y (2006) Two-step B-splines regularization method for solving an ill-posed problem of impact-force reconstruction. *Journal of Sound and Vibration* 297: 200–214.
- Hansen PC (1994) Regularization tools: a Matlab package for analysis and solution of discrete ill-posed problems. *Numerical Algorithms* 6: 1–35.
- Hansen PC (1998) *Rank-Deficient and Discrete Ill-Posed Problems: Numerical Aspects of Linear Inversion*. Philadelphia, PA: SIAM.
- Hu N, Fukunaga H, Matsumoto S, et al. (2007a) An efficient approach for identifying impact force using embedded piezoelectric sensors. *International Journal of Impact Engineering* 34: 1258–1271.
- Hu N, Matsumoto S, Nishi R, et al. (2007b) Identification of impact forces on composite structures using an inverse approach. *Structural Engineering and Mechanics* 27: 409–424.
- Ihn J-B and Chang F-K (2008) Pitch-catch active sensing methods in structural health monitoring for aircraft structures. *Structural Health Monitoring* 7: 5–19.
- Inman DJ (2001) *Engineering Vibration*. Upper Saddle River, NJ: Prentice Hall.
- Inoue H, Harrigan JJ and Reid SR (2001) Review of inverse analysis for indirect measurement of impact force. *Applied Mechanics Reviews* 54: 503–524.
- Jang BW, Lee YG, Kim JH, et al. (2012) Real-time impact identification algorithm for composite structures using fiber Bragg grating sensors. *Structural Control and Health Monitoring* 19: 580–591.
- Kalhari H, Ye L, Li Z, et al. (2015) Identification of location and magnitude of impact force on a composite sandwich structure with lattice truss core. In: *ASME 2015 international mechanical engineering congress and exposition*, Houston, Texas, USA, 13–19 November 2015, pp. V001 T001A023. American Society of Mechanical Engineers.
- Kalhari H, Ye L, Mustapha S, et al. (2014) Impact force reconstruction on a concrete deck using a deconvolution approach. In: *8th Australasian congress on applied mechanics: ACAM 8*, Melbourne, VIC, 25–26 November, pp. 763–771. Barton, ACT: Engineers Australia.
- Kalhari H, Ye L, Mustapha S, et al. (2016) Reconstruction and analysis of impact forces on a steel-beam-reinforced concrete deck. *Experimental Mechanics*.
- Kundu T, Das S and Jata KV (2007) Point of impact prediction in isotropic and anisotropic plates from the acoustic emission data. *Journal of the Acoustical Society of America* 122: 2057–2066.
- Li B, Ye L, Li Z, et al. (2015) Quantitative identification of delamination at different interfaces using guided wave signals in composite laminates. *Journal of Reinforced Plastics and Composites* 34: 1506–1525.
- Liljedahl C, Fitzpatrick M and Edwards L (2008) Residual stresses in structures reinforced with adhesively bonded straps designed to retard fatigue crack growth. *Composite Structures* 86: 344–355.
- Mao YM, Guo XL and Zhao Y (2010) Experimental study of hammer impact identification on a steel cantilever beam. *Experimental Techniques* 34: 82–85.
- Mustapha S and Ye L (2014) Leaky and non-leaky behaviours of guided waves in CF/EP sandwich structures. *Wave Motion* 51: 905–918.
- Mustapha S and Ye L (2015) Propagation behaviour of guided waves in tapered sandwich structures and debonding identification using time reversal. *Wave Motion* 57: 154–170.
- Mustapha S, Ye L, Dong X, et al. (2016) Evaluation of barely visible indentation damage (BVID) in CF/EP sandwich composites using guided wave signals. *Mechanical Systems and Signal Processing* 76: 497–517.
- Mustapha S, Ye L, Wang D, et al. (2012) Debonding detection in composite sandwich structures based on guided waves. *AIAA Journal* 50: 1697–1706.
- Park J, Ha S and Chang F-K (2009) Monitoring impact events using a system-identification method. *AIAA Journal* 47: 2011–2021.
- Peelamedu SM, Naganathan NG, Dukkupati RV, et al. (2005) Impact identification for a metallic plate using distributed smart materials. *Smart Materials and Structures* 14: 449–456.
- Qiao B, Zhang X, Luo X, et al. (2015) A force identification method using cubic B-spline scaling functions. *Journal of Sound and Vibration* 337: 28–44.
- Seydel R and Chang F-K (2001a) Impact identification of stiffened composite panels: I System development. *Smart Materials and Structures* 10: 354–369.
- Seydel R and Chang F-K (2001b) Impact identification of stiffened composite panels: II Implementation studies. *Smart Materials and Structures* 10: 370–379.
- Staszewski W, Mahzan S and Traynor R (2009) Health monitoring of aerospace composite structures – active and passive approach. *Composites Science and Technology* 69: 1678–1685.
- Thiene M and Galvanetto U (2015) Impact location in composite plates using proper orthogonal decomposition. *Mechanics Research Communications* 64: 1–7.
- Tracy M and Chang F-K (1998) Identifying impacts in composite plates with piezoelectric strain sensors, part I: theory. *Journal of Intelligent Material Systems and Structures* 9: 920–928.
- Tracy MJ and Chang F-K (1996) Identifying impact load in composite plates based on distributed piezoelectric sensor measurements. In: *Proceedings of the SPIE 2717, smart structures and materials 1996. International society for optics and photonics*, San Diego, CA, 25 February, pp. 231–236.
- Worden K and Staszewski W (2000) Impact location and quantification on a composite panel using neural networks and a genetic algorithm. *Strain* 36: 61–68.